

Use of Multiple Verification Methods to Evaluate Forecasts of Convection from Hot- and Cold-Start Convection-Allowing Models

DEREK R. STRATMAN

School of Meteorology, University of Oklahoma, Norman, Oklahoma

MICHAEL C. CONIGLIO AND STEVEN E. KOCH

NOAA/National Severe Storms Laboratory, Norman, Oklahoma

MING XUE

School of Meteorology, and Center for Analysis and Prediction of Storms, University of Oklahoma, Norman, Oklahoma

(Manuscript received 16 March 2012, in final form 14 August 2012)

ABSTRACT

This study uses both traditional and newer verification methods to evaluate two 4-km grid-spacing Weather Research and Forecasting Model (WRF) forecasts: a “cold start” forecast that uses the 12-km North American Mesoscale Model (NAM) analysis and forecast cycle to derive the initial and boundary conditions (C0) and a “hot start” forecast that adds radar data into the initial conditions using a three-dimensional variational data assimilation (3DVAR)/cloud analysis technique (CN). These forecasts were evaluated as part of 2009 and 2010 NOAA Hazardous Weather Test Bed (HWT) Spring Forecasting Experiments. The Spring Forecasting Experiment participants noted that the skill of CN’s explicit forecasts of convection estimated by some traditional objective metrics often seemed large compared to the subjectively determined skill. The Gilbert skill score (GSS) reveals CN scores higher than C0 at lower thresholds likely due to CN having higher-frequency biases than C0, but the difference is negligible at higher thresholds, where CN’s and C0’s frequency biases are similar. This suggests that if traditional skill scores are used to quantify convective forecasts, then higher (>35 dBZ) reflectivity thresholds should be used to be consistent with expert’s subjective assessments of the lack of forecast skill for individual convective cells. The spatial verification methods show that both CN and C0 generally have little to no skill at scales <8 – $12\Delta x$ starting at forecast hour 1, but CN has more skill at larger spatial scales (40–320 km) than C0 for the majority of the forecasting period. This indicates that the hot start provides little to no benefit for forecasts of convective cells, but that it has some benefit for larger mesoscale precipitation systems.

1. Introduction

Every spring, operational forecasters and research scientists participate in the National Oceanic and Atmospheric Administration’s (NOAA) Hazardous Weather Test Bed (HWT) Spring Forecasting Experiment, which is designed to improve communication and facilitate collaboration among forecasters and researchers through the generation of daily experimental convective forecasts and the evaluation of experimental forecast models

(Kain et al. 2010; Clark et al. 2012). For the 2009 and 2010 Spring Forecasting Experiments (SFE2009 and SFE2010, respectively), the Center for Analysis and Prediction of Storms (CAPS) at the University of Oklahoma produced ensemble forecasts at 4-km grid spacing, in nearly (in 2009) and fully (in 2010) conterminous U.S. (CONUS) domains, using the Weather Research and Forecasting Model (WRF; Xue et al. 2009, 2010). The ensemble forecasts were run once a day, starting from 0000 UTC on week days, and the length of forecasts was 30 h. Among the ensemble members for both years, two members of interest used the Advanced Research core of the WRF (WRF-ARW): one member directly used the 0000 UTC 12-km North American Mesoscale Model (NAM) analyses at the initial

Corresponding author address: Derek R. Stratman, National Weather Center, NSSL/FRDD, 120 David L. Boren Blvd., Norman, OK 73072.

E-mail: stratman@ou.edu

conditions and the other member used the three-dimensional variational data assimilation (3DVAR) cloud analysis (Xue et al. 2003; Hu et al. 2006a,b) initial conditions that assimilated radar and other high-resolution observations (from surface stations and wind profilers). The NAM analyses were used as the background. The two runs did not include additional initial condition perturbations and are referred to as two control runs—one with radar data (called CN) and one without radar data (called C0). The comparison between CN and C0 allows the evaluation of the impact of radar and other high-resolution data on the initial conditions, with radar data having a dominant effect given their relative data volume. All forecasts used NAM forecasts starting at the same initial times to provide the lateral boundary conditions. In addition to the 0000 UTC ensemble forecasts, CAPS was also producing forecasts over a smaller central U.S. domain, at 1200 UTC and several other times, using model configurations corresponding to those of 0000 UTC CN and C0 (except for the domain size). These runs were made to support the Second Verification of the Origins of Rotation in Tornadoes Experiment (VORTEX2; Xue et al. 2009, 2010). In this study, we will evaluate and initially compare the 0000 and 1200 UTC CN and C0 forecasts.

During 2009 and 2010, participants in the Spring Forecasting Experiment compared hourly loops of CN- and C0-simulated reflectivity (SR) forecasts to the observed radar reflectivity (OR) for the same time periods on a large monitor. They were asked to define when the cold-start forecasts (C0) appeared to “catch up” with the hot-start forecasts (CN) “in terms of its degree of correspondence with reality.” For SFE2009, nearly 60% of the participants perceived 0000 UTC CN forecasts to be effectively similar to the C0 forecasts in their depiction of convection after 3–6 h. For example, one participant commented, “by [forecast hours] 3–4 the two model runs tend to look more like each other than like the obs[ervations].” This sentiment is illustrated for an individual case in Fig. 1. At the initial time, CN’s SR looked very similar to the OR, which is the result of the reflectivity assimilation in the cloud analysis step. However, by forecast hour 3 and especially by forecast hour 6, the subjective impression of the participants is that both forecasts were equally skillful–unskillful in their forecasts of that convective event.

This study aims to complement the subjective assessment of CN’s and C0’s skill in forecasting convection discussed above by providing a comprehensive objective assessment of its skill. The skill is characterized through traditional metrics, as well as through newer techniques that define model errors by spatial scales and variable thresholds. The latter approach delineates the spatial scales at which CN improves over C0 and provides

a more comprehensive assessment of model skill over what can be provided by a subjective evaluation, or by traditional gridpoint-by-gridpoint techniques.

The HWT forecasting experiments have shown that subjective evaluations can provide valuable information on the tools that forecasters find useful, but they are limited in defining the specific error characteristics of numerical model forecasts that researchers strive to address. Simple quantitative verification techniques (that compare a forecast of some quantity to an analysis or observation of that quantity at specific points in space and time) have long been used to objectively evaluate model forecasts. As higher-resolution numerical models are now used to predict highly discontinuous fields, like convection, there is an increasing need in the research community to use newer verification techniques (Casati et al. 2008; Gilleland et al. 2009; Gilleland et al. 2010). Because traditional gridpoint-by-gridpoint verification metrics effectively give much weight to the smallest scales allowed by the gridded model forecasts and observations, small deviations (i.e., errors) in the model forecasts from the observations can often cause misrepresentation of the useful model forecast skill (i.e., skill a forecaster would deem useful and appropriate). Newer verification techniques that attempt to better characterize model skill for discontinuous fields can be classified into one of four categories: neighborhood (or fuzzy), scale-separation (or decomposition), feature based (or object based), and field deformation techniques (Gilleland et al. 2009). This study uses the first two types, which are different ways of evaluating model skill through a filtering of the gridded fields.

Several traditional verification metrics and two filtering techniques (described in section 3) are used in this study to analyze the performance of CN and C0 in an individual and a comparative sense. A goal of using these spatial-scale filtering methods is to determine if the spatial verification metrics are more consistent with the SFE2009 and SFE2010 participants’ subjective evaluations since the traditional verification scores are often not appropriate measures of skill for high-resolution model forecasts of discontinuous fields (Gilleland et al. 2009), like strong convection. Another goal of this study is to assess the benefit of the CAPS 3DVAR cloud analysis radar data assimilation technique (described in section 2), as applied to the CN forecasts.

2. Datasets

a. CAPS CN and C0 forecasts

As mentioned earlier, the two Advanced Research WRF (WRF-ARW) model runs examined in this study

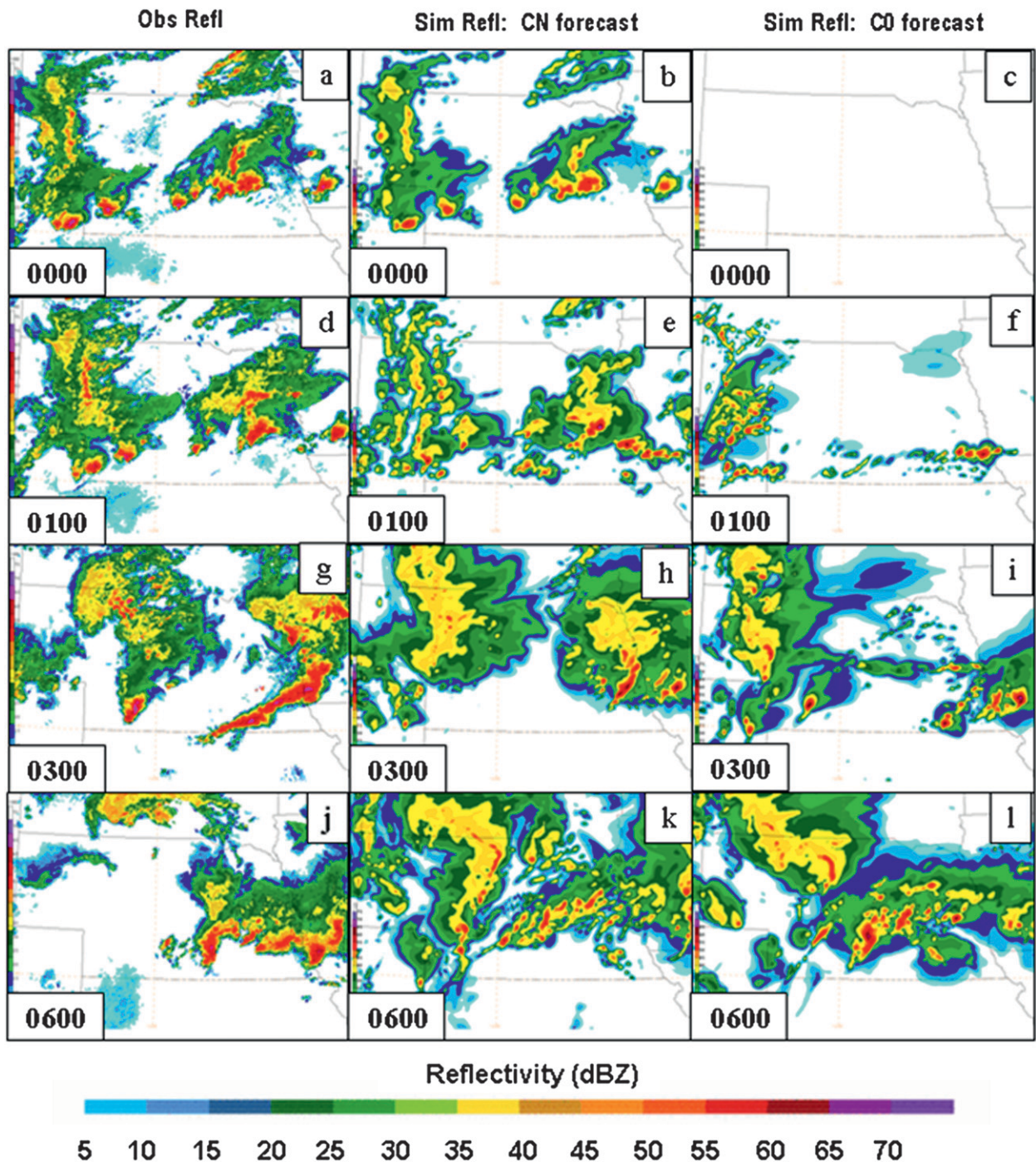


FIG. 1. (left) Observed composite (column maximum) reflectivity and 0000 UTC initialized simulated composite reflectivity from CAPS (middle) CN and (right) C0 at 0000, 0100, 0300, and 0600 UTC 5 Jun 2008 (from Kain et al. 2010).

were part of the CAPS 4-km grid-spacing Storm Scale Ensemble Forecast (SSEF) system run in the springs of 2009 and 2010 (see Xue et al. 2009, 2010 for specific details). The 2009 version of the SSEF system was composed of 10 WRF-ARW members, 8 Nonhydrostatic

Mesoscale Model (WRF-NMM) members, and 2 Advanced Regional Prediction System (ARPS) members, while the 2010 SSEF system contained 19 WRF-ARW members, 5 WRF-NMM members, and 2 ARPS members. For SFE2009, the 0000 UTC WRF-ARW control

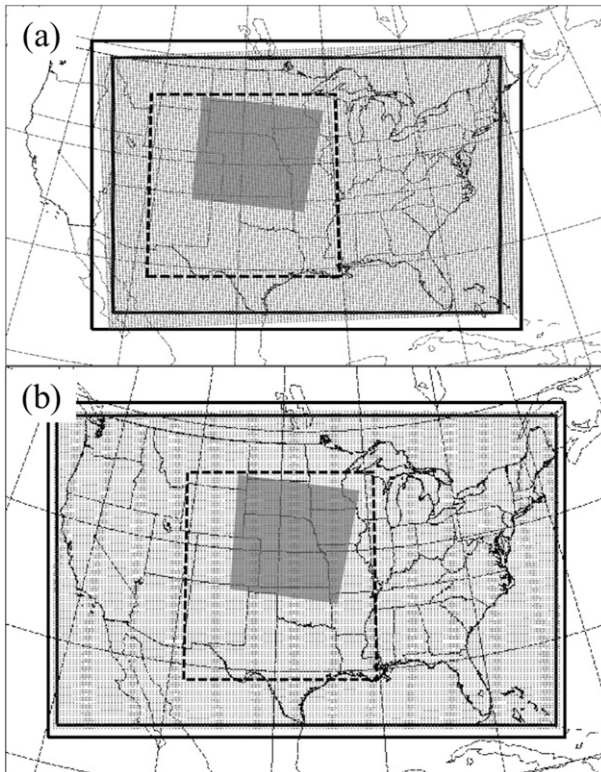


FIG. 2. The inner bold box is the domain for 0000 UTC WRF-ARW with (a) 900×672 grid points in 2009 and (b) 999×790 grid points in 2010, and the outer bold box is the somewhat larger ARPS 3DVAR analysis domain. The inner dashed box is the 1200 UTC model domain for both years (444×480 grid points). The gray-shaded polygon is an example “VORTEX2” moveable domain with 256×256 horizontal grid points used for verification (see Xue et al. 2009, 2010).

members (i.e., CN and C0) were integrated to 30 h on an eastern near-CONUS-size domain (Fig. 2a). For SFE2010, CN and C0 were once again integrated to 30 h starting at 0000 UTC, but the domain increased to a full CONUS-size domain (Fig. 2b). For both SFE2009 and SFE2010, the 1200 UTC CN and C0 members were integrated to 18 h on the central Great Plains domain (Figs. 2a,b).

CN assimilates radar radial velocity with a mass divergence constraint in the 3DVAR procedure to derive the wind components for the initial conditions in combination with the NAM background and additional surface and wind profiler data (Hu et al. 2006b). In addition, CN uses a cloud analysis scheme, which adds hydrometeors and adjusts the in-cloud temperature and moisture fields through a moist-adiabatic scheme using three-dimensional radar reflectivity data as well as surface cloud-base and satellite cloud-top observations (Xue et al. 2003; Hu et al. 2006a). Except for the initial conditions, all other model configurations [i.e., boundary conditions from the NAM fields, Thompson cloud

microphysics scheme, Goddard shortwave radiation physics, Rapid Radiative Transfer Model (RRTM) long-wave radiation physics, Noah land surface model, and Mellor–Yamada–Janjić planetary boundary layer physics] are identical between CN and C0 (Xue et al. 2009; 2010).

The 0000 and 1200 UTC model runs are examined separately. Combining both years yielded a maximum 56 days of data for the 0000 UTC model runs and 77 days of data for the 1200 UTC model runs (the 1200 UTC forecasts were run on weekends also). These datasets are used to evaluate and compare the models’ hourly SR and 1-h accumulated precipitation (APCP) fields.

b. Verification data and domain

Composite reflectivity and quantitative precipitation estimates calculated on a 1-km grid as part of the National Severe Storms Laboratory (NSSL) National 3D Reflectivity Mosaic system are used for the verifying observations (see Vasiloff et al. 2007 for more details). Even though the 0000 UTC forecasts were performed on large CONUS-sized domains, this study focuses on the central Great Plains region that was the focus of the VORTEX2 field experiment during the two spring seasons. Given that the wavelet scale-separation method used in this study requires domains to be $2^n \times 2^n$ grid points in size (see section 3c) and given the 4-km grid spacing of the model forecasts, a reasonably sized verification domain was chosen to be made up of 256×256 grid points in the horizontal ($n = 8$) given the smaller size of the 1200 UTC domain. Because the model forecasts and verification fields were on different native grids, prior to verification, the fields were interpolated onto a 256×256 portion of the AWIPS 240 grid (following Schwartz et al. 2009), which has a horizontal grid spacing of 4.7625 km.

Due to its small size relative to the model domains, the verification domain was moveable¹ (Fig. 2) to follow areas where observed convection occurred. If no convection occurred on a particular day, the domain was centered on Norman, Oklahoma. In addition, the western edge of the domain always had a longitude of 105°W , so the domain moved north and south to follow active areas of convection over the central United States.

3. Verification metrics

a. Traditional scores

Using thresholds of 10, 20, 30, and 40 dBZ for SR and 0.1, 1.0, 5.0, and 10.0 mm h^{-1} for APCP, standard 2×2

¹ It is worth noting as a caveat that the climatology varies as the verification domain is moved from location to location (Hamill and Juras 2006).

contingency table components (i.e., hits, false alarms, misses, and correct negatives) were generated hourly for forecast hours 0–12 for each model run using version 3.0 of the Model Evaluation Tools (MET), which was developed and is currently maintained by NOAA/National Center for Atmospheric Research (NCAR) through the Development Test Bed Center (DTC 2011). All of the individual components of the contingency tables for each model–threshold combination were summed using MET to form contingency tables for each forecast hour. From these summed contingency tables, four traditional metrics were computed: frequency bias (FBIAS), probability of detection (POD), probability of false detection (POFD), and Gilbert skill score (GSS) (otherwise known as the equitable threat score or ETS). Confidence intervals (CI) of 95% were included for each metric for each forecast hour to assess the uncertainty in the estimates following the resampling procedure of Hamill (1999). The CIs are assigned in a comparative sense; the uncertainty in the difference in the metrics between the two model forecasts in question is assessed by computing CIs on the metric differences at each forecast hour. If the CIs on the difference estimates include the zero line for a particular forecast hour, the differences of the verification metrics are said to be not significantly different, and vice versa.

b. Neighborhood method

Using the neighborhood method based on Roberts and Lean (2008), the fractions skill score (FSS) is computed to assess the skill for different neighborhood sizes and variable thresholds. The neighborhood method allows for a “hit” to be within a certain neighborhood (radius) of the observation, which allows for forecasts that are “close enough” to be considered skillful in the objective metrics (Ebert 2008, 2009). FSS ranges from 0 for no skill to 1 for perfect skill, as given by

$$\text{FSS} = 1 - \frac{\frac{1}{N} \sum (P_{\text{fcst}} - P_{\text{obs}})^2}{\frac{1}{N} \left(\sum P_{\text{fcst}}^2 + \sum P_{\text{obs}}^2 \right)}, \quad (1)$$

where P_{fcst} and P_{obs} are the fractional forecast and observed SR (or ACP) areas in each neighborhood that exceed the specified variable threshold and N is the number of neighborhoods for each neighborhood size. (Note: larger neighborhood sizes lead to a smaller number of neighborhoods, whereas smaller sizes will result in a larger N .) In an evaluation of precipitation forecasts from convection-allowing models, Roberts and Lean (2008) estimated that forecasts have useful skill ($\text{FSS}_{\text{useful}}$) when $\text{FSS}_{\text{useful}} = 0.5 + f_o/2$, where f_o is the

base rate, or fraction of observed events to all grid points. They consider this value to be a reasonable “target skill” since it is halfway between the random forecast skill and perfect skill. This same value for $\text{FSS}_{\text{useful}}$ is used in this study, and forecasts for which $\text{FSS} > \text{FSS}_{\text{useful}}$ are considered to have useful skill.

An aggregated FSS^2 was computed for each forecast hour for neighborhood widths, n , of 1, 3, 5, 9, 17, 33, and 65 grid points centered at the grid box in question. For each neighborhood width, FSS was calculated for different SR and ACP thresholds (i.e., 10, 15, 20, 25, 30, 35, 40, 45, and 50 dBZ and 0.1, 0.5, 1.0, 2.5, 5.0, 7.5, 10.0, 20.0, and 40.0 mm h⁻¹, respectively). The aggregated $\text{FSS} - \text{FSS}_{\text{useful}}$ is displayed in a matrix of neighborhood size versus a variable threshold for a particular forecast hour for the individual neighborhood size and threshold combinations. Whenever $\text{FSS} - \text{FSS}_{\text{useful}}$ is positive, the forecast is considered to have useful skill. In addition, similar plots are shown for the differences in FSS between the models along with 95% confidence intervals, which were computed again following the procedure of Hamill (1999).

c. Scale-separation method

Like the neighborhood method, scale-separation methods allow for nonoverlapping forecasts and observations to be considered skillful in the objective metrics, but have the additional benefit of assessing the skill at individual, independent spatial scales of the errors (Casati et al. 2004). The particular intensity-scale verification (ISV) technique employed in this study is based on Casati et al. (2004), which isolates the skill at scales given by $2^l \times 2^l$ for $l = 0, 1, 2, \dots, 8$, where $l = 0$ represents the horizontal spacing of one grid cell (4.7625 km) and $l = 8$ represents the entire verification domain (1219 km \times 1219 km). This study retains the biases in the forecasts, as in Casati (2010), to also assess the bias associated with the various spatial scales and thresholds.

The first step is to transform forecast and observation fields into binary fields based on variable thresholds. The same variable thresholds used for the neighborhood method were also used for this method. A 2D Haar wavelet decomposition is then performed on the binary difference images between the forecasts and observations (i.e., the binary difference images are decomposed into scale components in this step; see Fig. 3 for an example

² For each forecast hour, the datasets were aggregated (Mittermaier and Roberts 2010) together for each combination of neighborhood width and threshold. Knowing the FBS, FSS, and N values, the summations in the numerator and denominator of Eq. (1) were calculated and aggregated separately for the individual datasets. The aggregated summations were then used to calculate FSS.

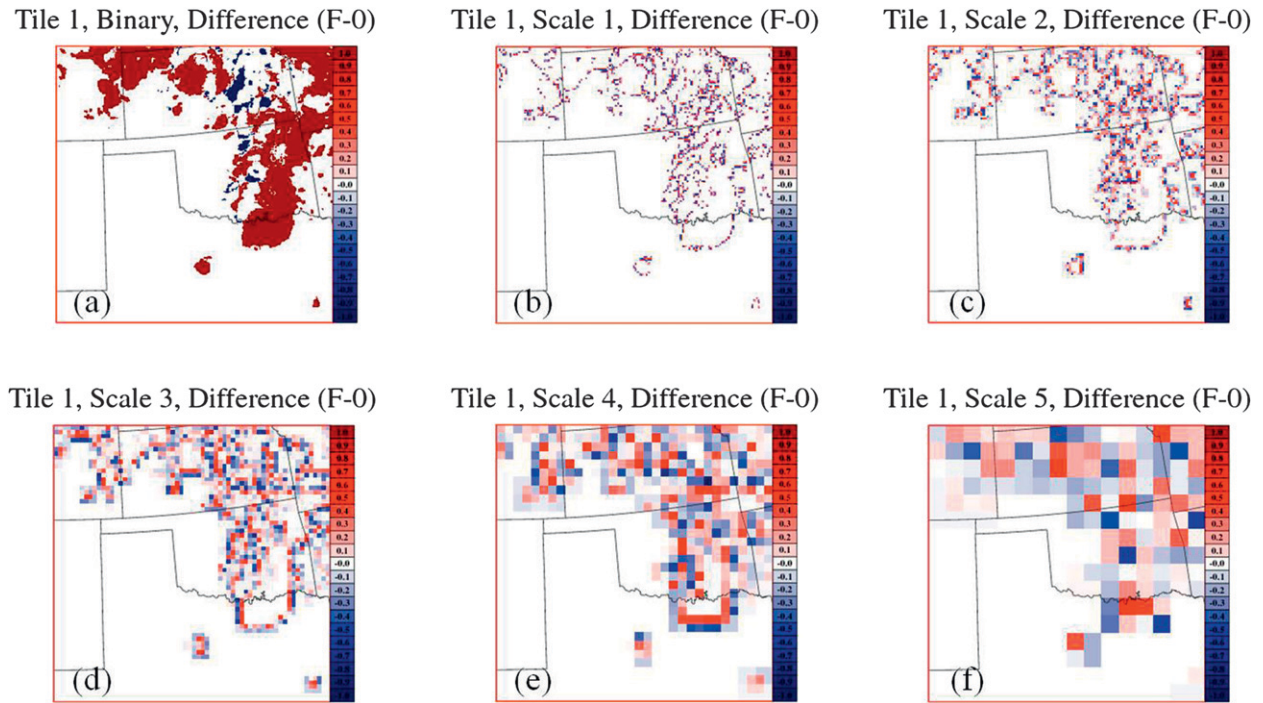


FIG. 3. (a) Example of a binary difference field, where the blue shading represents misses, the red shading represents false alarms, and the white areas represent hits and correct negatives, of simulated reflectivity ≥ 20 dBZ, for (b) scale 1, (c) scale 2, (d) scale 3, (e) scale 4, and (f) scale 5 components for 1500 UTC 10 May 2010 CAPS CN at FH 8. A major tornado outbreak occurred from the afternoon into the evening in central-eastern OK and KS.

of a binary difference field and its first five scale components). Next, a mean squared error (MSE) of the scale components of the binary field difference is calculated for each threshold and scale component. Because the sum of MSE from the individual scale components is equal to the MSE of the binary difference field image, the errors of individual scales can be examined separately (Casati et al. 2004).

To generate a baseline skill, a random MSE term is defined using the equation

$$\text{MSE}_{\text{random}} = \text{FBIAS} \times \text{BR} \times (1 - \text{BR}) + \text{BR} \times (1 - \text{FBIAS} \times \text{BR}), \quad (2)$$

where FBIAS is the frequency bias and BR is the base rate (Casati 2010). A skill score is defined for each binary forecast and observation scale component, called the intensity scale skill (ISS) score, and is given by

$$\text{ISS} = 1 - \frac{\text{MSE}}{\text{MSE}_{\text{random}}/(L + 1)}, \quad (3)$$

where $L = 8$ for this study. Positive ISS values are associated with skillful forecasts and negative ISS values are associated with forecasts with no skill (Casati 2010). Typically, large weather features, such as frontal convection,

are fairly well forecasted by convection-allowing models, so the larger spatial scales tend to exhibit positive skill. Conversely, small-scale weather features, such as individual convective cells, are not usually forecast well by the same convection-allowing models due to their general inability to resolve features less than $\sim 4\text{--}8\Delta x$ and the generally faster error growth at shorter wavelengths, so the smaller spatial scales tend to exhibit little to no forecasting skill. Plots of the ISS scores were created similar to the plots of the FSS values with thresholded values on the abscissa and the spatial scale on the ordinate, corresponding to $l = 0, 1, 2, 3, 4, 5$, and 6 in the wavelet transform application. In addition, plots of the difference (and their statistical significance) in ISS between models were created to assess the models' differences.

Finally, the energy was assessed for both the forecast and observation for each scale component and threshold through the evaluation of the energy squared ($\text{En}2$) quantities (Casati 2010). For variable X , $\text{En}2$ is given by

$$\text{En}2(X) = \frac{1}{N} \sum_{i=1}^N X_i^2, \quad (4)$$

where N is the total number of wavelet cells in the domain and X_i is the average of the gridpoint-squared

values in the i th grid cell. For high-resolution NWP models, in general, high energy is associated with small thresholds because of the relatively large number of events exceeding the threshold value, and conversely, low energy is associated with large thresholds because of the relatively small number of events exceeding the threshold value (Casati 2010). The bias is then assessed by comparing the $\text{En}2(F)$ and $\text{En}2(O)$ values with each other for every threshold and spatial scale by computing the energy (squared) relative difference (ERD):

$$\text{ERD} = \frac{[\text{En}2(F) - \text{En}2(O)]}{[\text{En}2(F) + \text{En}2(O)]}. \quad (5)$$

The ERD values range from -1 to 1 . Positive ERD values indicate overforecasting (a high bias), and negative ERD values indicate underforecasting (a low bias) (Casati 2010).

4. Results

a. Traditional metrics

According to the GSS, the 0000 UTC CN scored better than C0 for all forecast hours at the 20-dBZ threshold at the 5% significance level (Fig. 4a). However, while significance exists at the 5% level for all forecast hours, the lower bound of the 95% confidence interval is close to zero beyond forecast hour (FH hereafter) 5, so no strong conclusions can be drawn at those hours. Similar conclusions can be reached from looking at the GSS derived from the APCP field for the 1.0-mm threshold (Fig. 4c). This similarity between the SR and APCP verification scores of comparable thresholds was a common theme for all of the results found in this study, so only the verification scores for the SR fields are shown hereafter to eliminate redundancy.

At the 40-dBZ threshold (Fig. 4b), CN's GSS values remain above those of C0, but the difference quickly decreases in the first 2 h; the differences are barely significant at the 5% level from FH 2 to 4 and lack significance beyond FH 4. This indicates a much more rapid drop in relative skill between the two models for the higher threshold. In addition, the scores themselves are not much better than what could be achieved at random with scores that drop and remain below a GSS of 0.1 at the first forecast hour for CN. These results indicate that the model is having a hard time accurately evolving, usually small-scale, high-reflectivity cores that are initialized from the radar reflectivity observations. Both inadequate resolution and less than optimal analysis of

the intense convection in the initial conditions coupled with intrinsic faster error growth at small scales can cause such a fast drop in skill score.

At the 20-dBZ threshold for the 1200 UTC model runs (Fig. 5a), the differences in GSS between CN and C0 are somewhat smaller than they are for the 0000 UTC runs; they become statistically insignificant at the 95% confidence level around FH 4–5. The smaller differences in scores between CN and C0 for the 1200 UTC runs may be related to the diurnal cycle of convection. Convection is typically more abundant at 0000 UTC than at 1200 UTC, so CN has an initial benefit of assimilating more radar data into the initial conditions than is assimilated at 1200 UTC. Furthermore, the areal coverage of convection in the spring and summer tends to peak after 0000 UTC in the plains and tends to be much less during the 1200–1800 UTC period (Wallace 1975; Easterling and Robinson 1985). GSS (and other traditional scores) is dependent on the base rate (i.e., higher base rate leads to larger GSS and lower base rate leads to smaller GSS) (Stephenson et al. 2008), so GSS will be larger for the forecasts with more observed convection. For the remainder of the analysis, the results for the 1200 UTC runs are qualitatively similar to those detailed for the 0000 UTC runs, so only the results for the 0000 UTC runs are shown for brevity.

The forecast hour at which the GSSs for CN and C0 converge drops from about FH 6–12 for the 20-dBZ threshold to about FH 2–3 for the 40-dBZ threshold for both the 0000 and 1200 UTC runs (Figs. 4b and 5b). This convergence of GSS for the higher thresholds generally agrees with the perceptions of the Spring Forecasting Experiment participants, who thought CN and C0 were usually equally skillful between about FH 3 and FH 6 upon an hourly visual inspection of the SR fields. A possible reason for this sentiment might have to do with color psychology. For example, humans perceive some objects that are yellow and red (≥ 35 -dBZ objects) to be dangerous (i.e., stop signs and red lights), while objects that are green and blue (< 35 -dBZ objects) are perceived as not dangerous (Elliot and Maier 2007; Lichtenfeld et al. 2009). Hence, the Spring Forecasting Experiment participants' eyes may have focused on reflectivities greater than 35 dBZ in the Spring Forecasting Experiment displays (see Fig. 1 for an example of the standard reflectivity color bar), and therefore gave the more intense convection greater weight than the larger areas of lighter precipitation in their subjective assessment of skill.

The comparison of the objective scores with the subjective evaluations suggests that the use of GSS at higher thresholds is preferred over the use of GSS at lower SR thresholds in an evaluation of model forecasts of

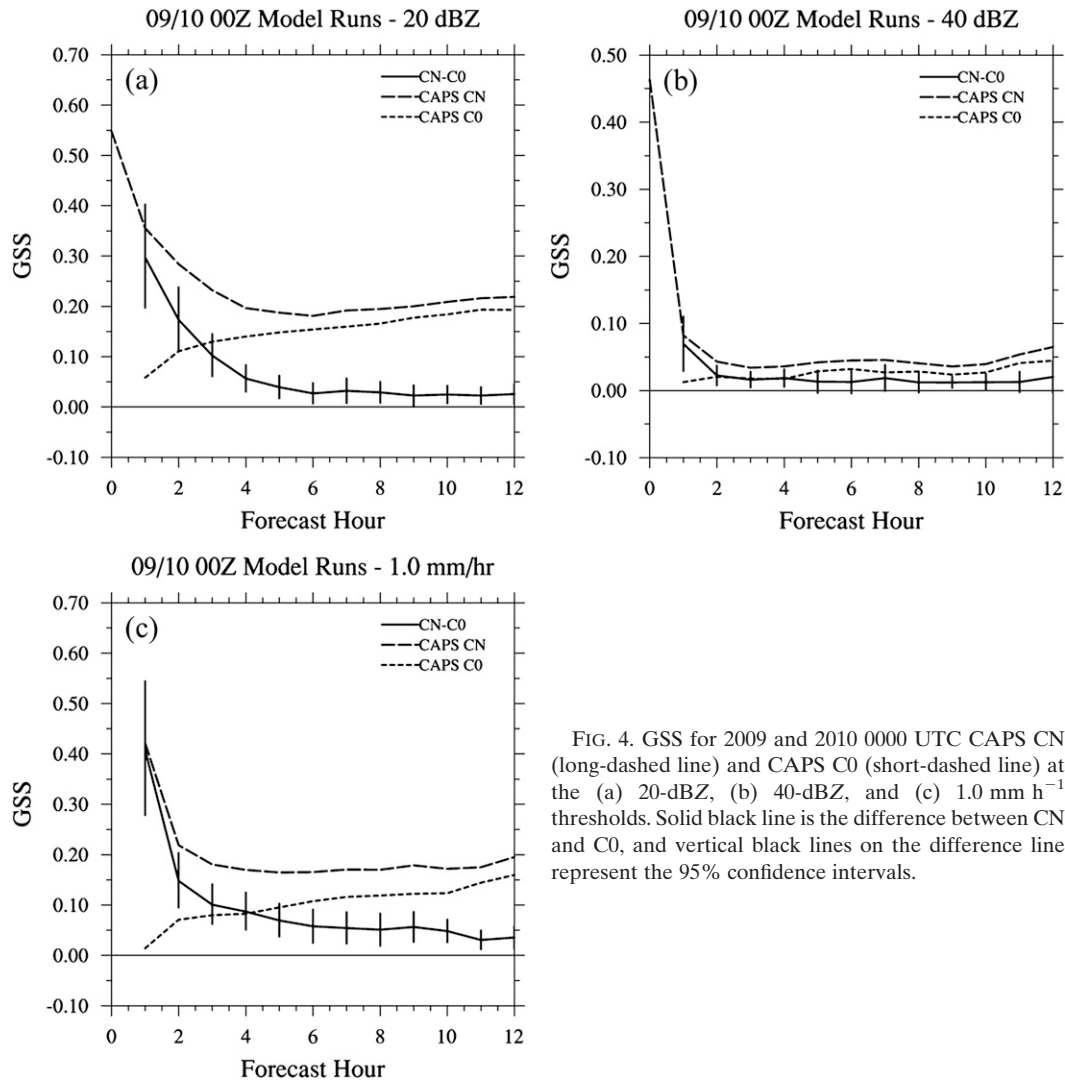


FIG. 4. GSS for 2009 and 2010 0000 UTC CAPS CN (long-dashed line) and CAPS C0 (short-dashed line) at the (a) 20-dBZ, (b) 40-dBZ, and (c) 1.0 mm h⁻¹ thresholds. Solid black line is the difference between CN and C0, and vertical black lines on the difference line represent the 95% confidence intervals.

convection because the conclusions based on the GSS values at higher thresholds are more consistent with the subjective conclusions than the conclusions based on the GSS values at lower thresholds. The GSS values for CN and C0 at these higher reflectivity thresholds are relatively low compared to typical GSS values of other model fields on coarser grids (likely due to the dependency of the GSS on the base rate), suggesting the model forecasts have relatively little forecasting skill for stronger convection. However, a more general point to be made is that the relative importance of CN and C0, as measured by the GSS, is highly dependent on the chosen reflectivity (or precipitation) threshold. Therefore, the use of a single metric like the GSS at any threshold can easily lead to a misrepresentation of model

performance for convection-allowing models (Doswell et al. 1990).

Another problem with the GSS arises due to high-frequency biases.³ In Fig. 6a, the frequency bias of the 0000 UTC initialized CN approaches a value of 2 by FH 2 and remains above 1.5 for the rest of the forecast period. For rare events, many traditional gridpoint-by-gridpoint scores, such as the GSS, are maximized for frequency biases >1 since these scores

³ Frequency biases are highly dependent on what microphysical scheme is used in a model, so it should be noted that these bias results and their effects on verification metrics are specific only to these models (i.e., different findings might result if different cloud microphysics schemes are used).

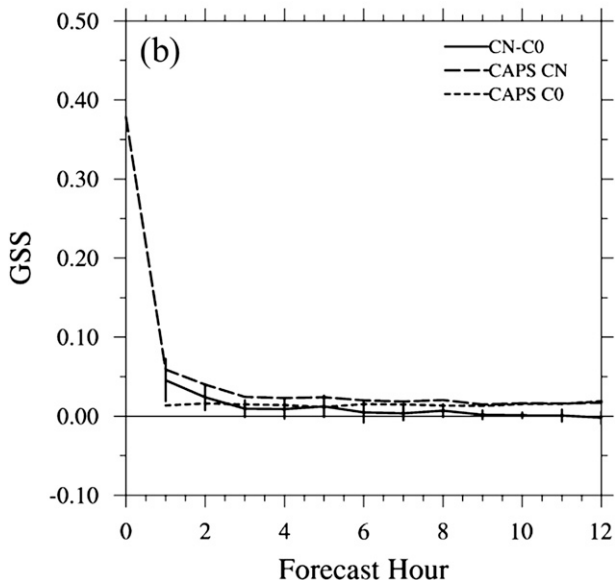
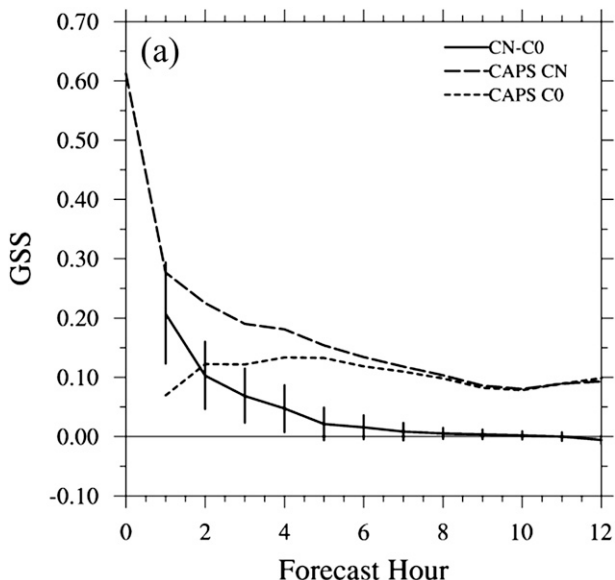


FIG. 5. As in Figs. 4a and 4b, but for 1200 UTC CAPS CN and CAPS C0.

are more sensitive to missed events than false alarms (Baldwin and Kain 2006). In other words, CN's high bias likely resulted in the noticeable improvement in the GSS for CN versus C0 for the 20-dBZ threshold. The differences in FBIAS between CN and C0 lead to higher POFD for CN for several hours, particularly for the 20-dBZ threshold (Figs. 6 and 7). The fact that CN has a higher FBIAS (and higher POFD) than C0 for the first few hours is not surprising since C0 is spinning up convection. However, the higher 20-dBZ FBIAS for CN persists through about FH 8 for the 0000 UTC runs (Fig. 6a), so the differences in FBIAS,

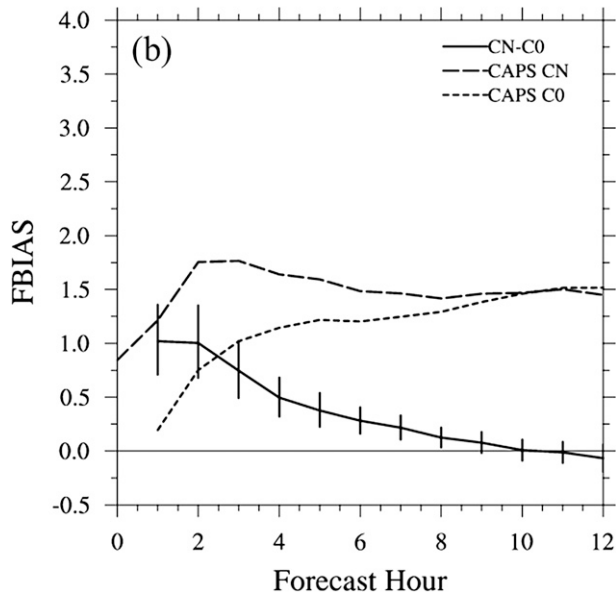
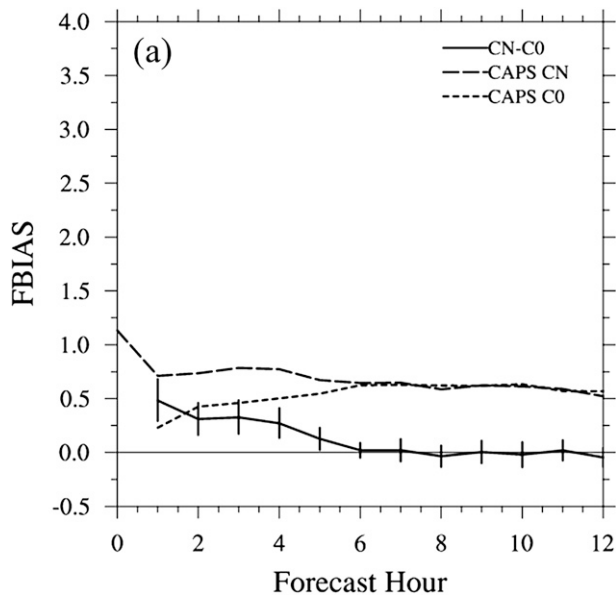


FIG. 6. As in Figs. 4a and 4b, but for frequency bias (FBIAS).

and the effects⁴ on the GSS, appear to linger after C0 spins up convection. This relationship in FBIAS and POFD between CN and C0 also is seen at the 40-dBZ threshold (Figs. 6b and 7b), although the FBIAS values and their differences are not as large.

b. Neighborhood method results

The previous section shows that a wide range of conclusions can be drawn about a model's performance

⁴ The bias-adjusted GSS from Mesinger (2008) was computed (not shown) and depicted smaller differences between CN and C0 through FH 6–8.

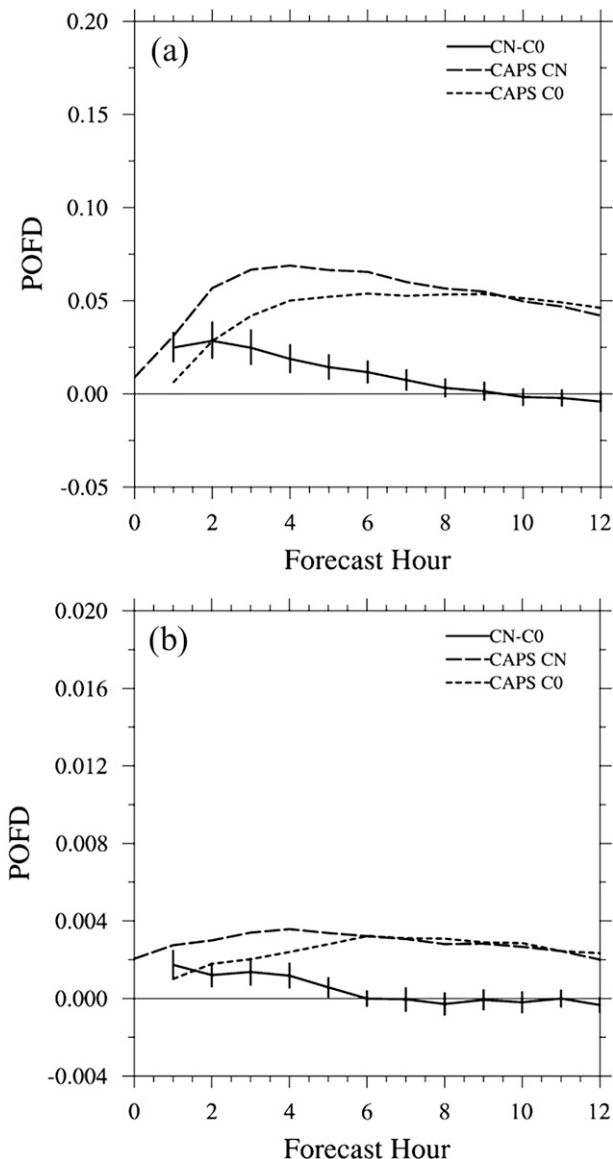


FIG. 7. As in Figs. 4a and 4b, but for POFD.

when using traditional gridpoint-by-gridpoint metrics computed from 2×2 contingency tables on explicit model forecasts of convection, depending on which threshold and metric are used for evaluation. Although some scores may underpenalize model forecasts if model biases are not accounted for, the lack of an overlay of forecasts and observations at the grid scale for highly discontinuous fields can overpenalize the forecasts and misrepresent the skill and usefulness of the forecasts, which may be the case for the 40-dBZ threshold GSS scores shown earlier. For the neighborhood metrics that attempt to account for forecasts that are “close enough,” not surprisingly, CN exhibits positive skill for all neighborhood sizes and reflectivity thresholds at the

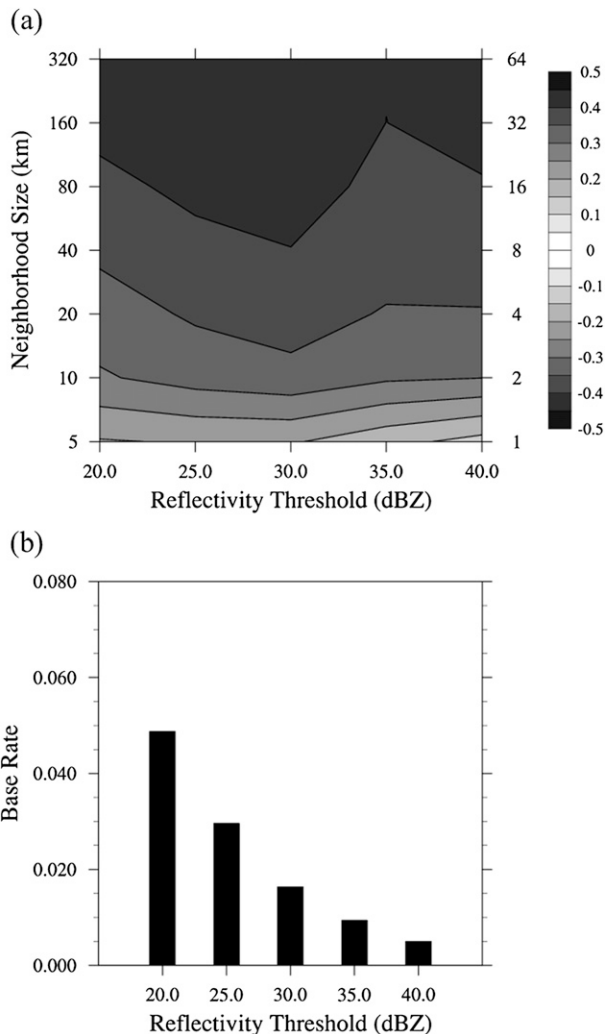


FIG. 8. (a) $FSS - FSS_{\text{useful}}$ for 2009 and 2010 for 0000 UTC CAPS CN at FH 0 for reflectivity thresholds every 5 dBZ from 20 and 40 dBZ and for neighborhood sizes from 5 to 320 km. Gray shading with solid contours represents useful skill, and gray shading with dashed contours (not depicted here) represents nonuseful skill. Values along the right ordinate represent multiples of the grid spacing. (b) Base rates of observed reflectivity for each threshold.

initial analysis time for the 0000 UTC initialization time (Fig. 8a). Again, this is because the hydrometeor fields are effectively inserted directly onto the native 4-km grid of the CN model through the cloud analysis scheme. Not surprisingly, the base rates⁵ decrease with increasing thresholds (Fig. 8b).

By FH 1 however, the 0000 UTC CN quickly loses useful skill at higher thresholds. Forecasts at the 30-dBZ

⁵ The base-rate bar graphs will be excluded from the results and discussion from this point forward, but they will be included in the figures for the reader’s interest.

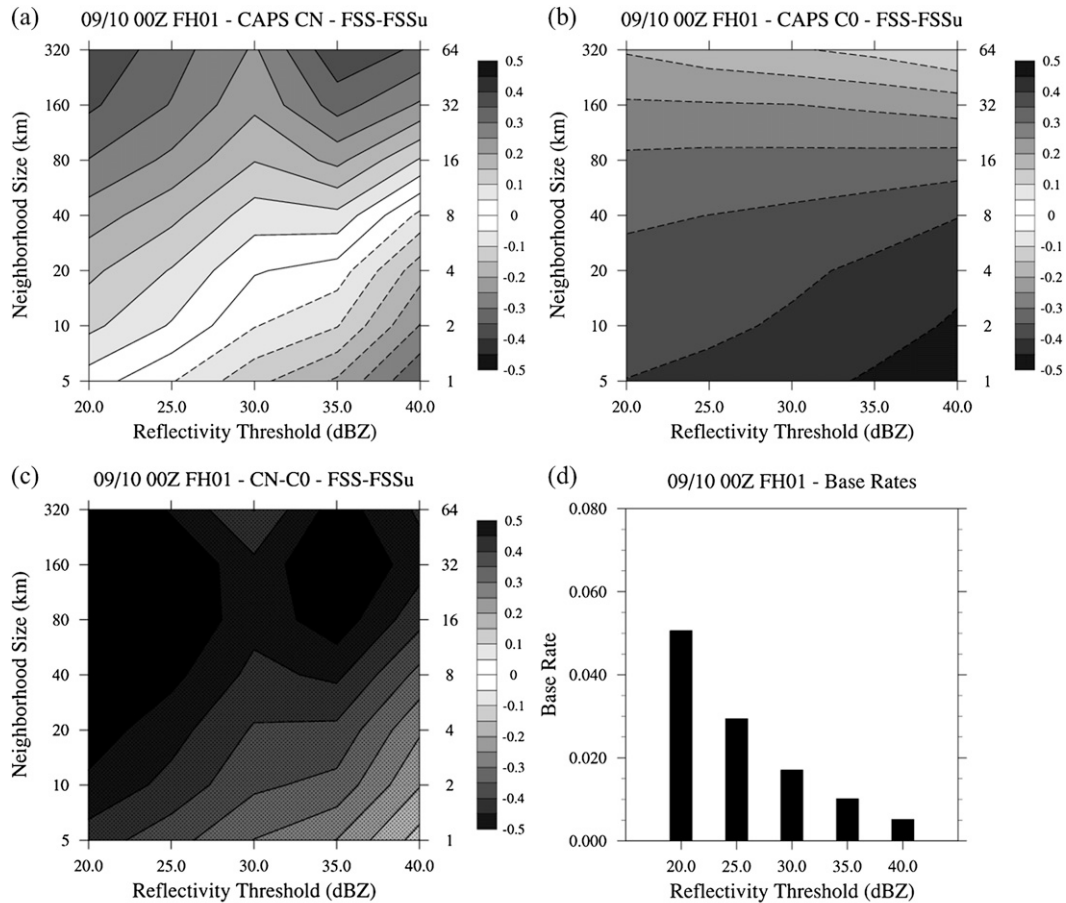


FIG. 9. FSS-FSS_{useful} for 2009 and 2010 for 0000 UTC (a) CAPS CN and (b) CAPS C0 at FH 1 for reflectivity thresholds every 5 dBZ from 20 and 40 dBZ and for spatial scales from 5 to 320 km. Gray shading with solid contours represents useful skill, and gray shading with dashed contours represents nonuseful skill. (c) Differences between CN and C0, where gray shading with solid contours represents FSSCN > FSSC0, gray shading with dashed contours (not depicted in these plots) represents FSSCN < FSSC0, and stippling depicts the 95% confidence interval (note that significance exists for all sizes and thresholds). Values along the right ordinate represent multiples of the grid spacing. (d) Base rates of observed reflectivity for each threshold.

threshold lose skill up to the 20-km neighborhood ($\sim 4\Delta x$) and the forecasts at the 40-dBZ threshold lose skill up to the 60-km neighborhood ($\sim 12\Delta x$) (Fig. 9a). In effect, the 0000 UTC CN model runs lose forecasting skill for small mesoscale and convective-scale neighborhoods, meaning they have little to no skill in the placement of individual convective cells and small convective clusters, after 1 h of integration. For comparison, C0 exhibits no useful skill for all depicted scales and thresholds for both model initialization times (Fig. 9b), but this is not surprising since C0 is still spinning up convection for the first few forecast hours. Although the dropoff in skill for CN is rapid, CN still outperforms C0 for all neighborhood and threshold combinations at FH 1 (Fig. 9c). The neighborhoods and reflectivity thresholds at which the alleviation of the spinup problem is

skillful are limited to neighborhoods greater than 5–10 km for the lower reflectivity thresholds (i.e., 20–30 dBZ) and neighborhoods greater than 20–40 km for the higher thresholds (i.e., 35–40 dBZ). Similarly, CN continues to outperform C0 at FH 2 and is, thus, not shown.

By FH 3, the 0000 UTC CN model runs continue to lose useful skill. The 0000 UTC CN model runs have useful skill for neighborhoods greater than ~ 30 km at the 20-dBZ threshold and for neighborhoods greater than ~ 140 km at the 40-dBZ threshold (Fig. 10a). Conversely, C0 gains useful skill for neighborhoods greater than ~ 150 km at the 20-dBZ threshold and for neighborhoods greater than ~ 310 km at the 40-dBZ threshold (Fig. 10b). CN continues to have greater skill than C0 at FH 3 (Fig. 10c), but the magnitude of the differences is decreasing.

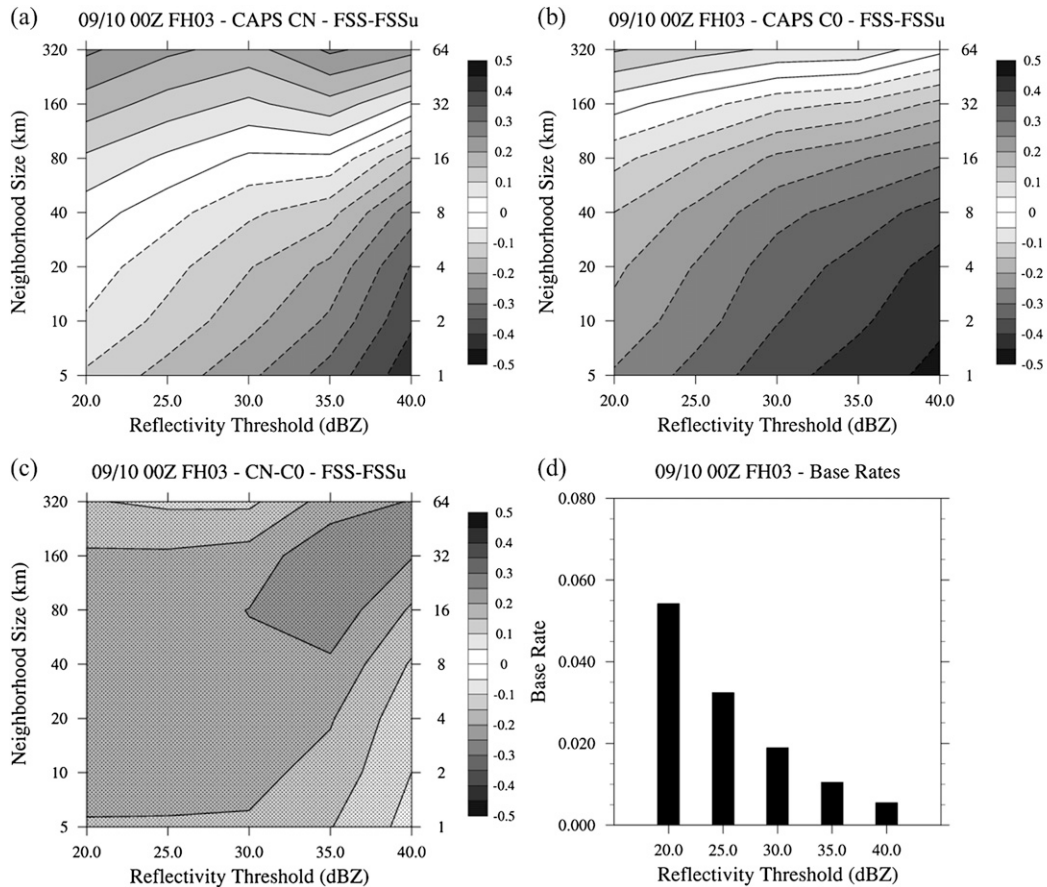


FIG. 10. As in Fig. 9, but for FH 3.

At FH 6, the 0000 UTC CN model runs maintain useful skill for neighborhoods greater than ~ 90 km at the 20-dBZ threshold and for neighborhoods greater than ~ 140 km at the 40-dBZ threshold (Fig. 11a), which is similar to the results at FH 3. Useful skill exists for neighborhoods greater than ~ 150 km at the 20-dBZ threshold and for neighborhoods greater than ~ 320 km at the 40-dBZ threshold for the 0000 UTC C0 model runs (Fig. 11b). The magnitude of the difference in skill between CN and C0 continues to decrease by FH 6, but are deemed to be significant at most neighborhoods and thresholds (Fig. 11c). At forecast hours 9 and 12, the results are similar to FH 6 and, thus, are not shown.

c. Scale-separation method results

Although the neighborhood method effectively weights small distance errors less and less as the size of the neighborhood increases, it does not define the contribution of specific spatial scales to the error (nor to their biases). The scale-separation method is able to isolate these scales. Furthermore, the scale-separation results give another perspective on where in the reflectivity–spatial-scale

parameter space the “useful skill” exists through the ISS. This additional information of useful skill is revealing because the FSS_{useful} used earlier may not be the optimal measure of useful skill.

For the initial analysis time, CN exhibits positive skill (positive ISS values are considered to define “useful skill” for the purpose of this study) for all spatial scales at thresholds less than 25 dBZ and for spatial scales greater than ~ 10 km at the 40-dBZ threshold (Fig. 12a⁶), so even for the initial hour, CN struggles with analyzing the amplitude of the higher-reflectivity cores. This is likely due to a somewhat smoothed representation of convection produced by the cloud analysis schemes. Even though CN is largely unbiased at the initial time, it is initialized with too much coverage of higher reflectivities for large spatial scales based on ERD values greater than 0.2 (Fig. 12b).

⁶ The left ordinate in the ISS plots represents the spatial scale of the binary forecast errors and not just the neighborhood size as for the neighborhood method.

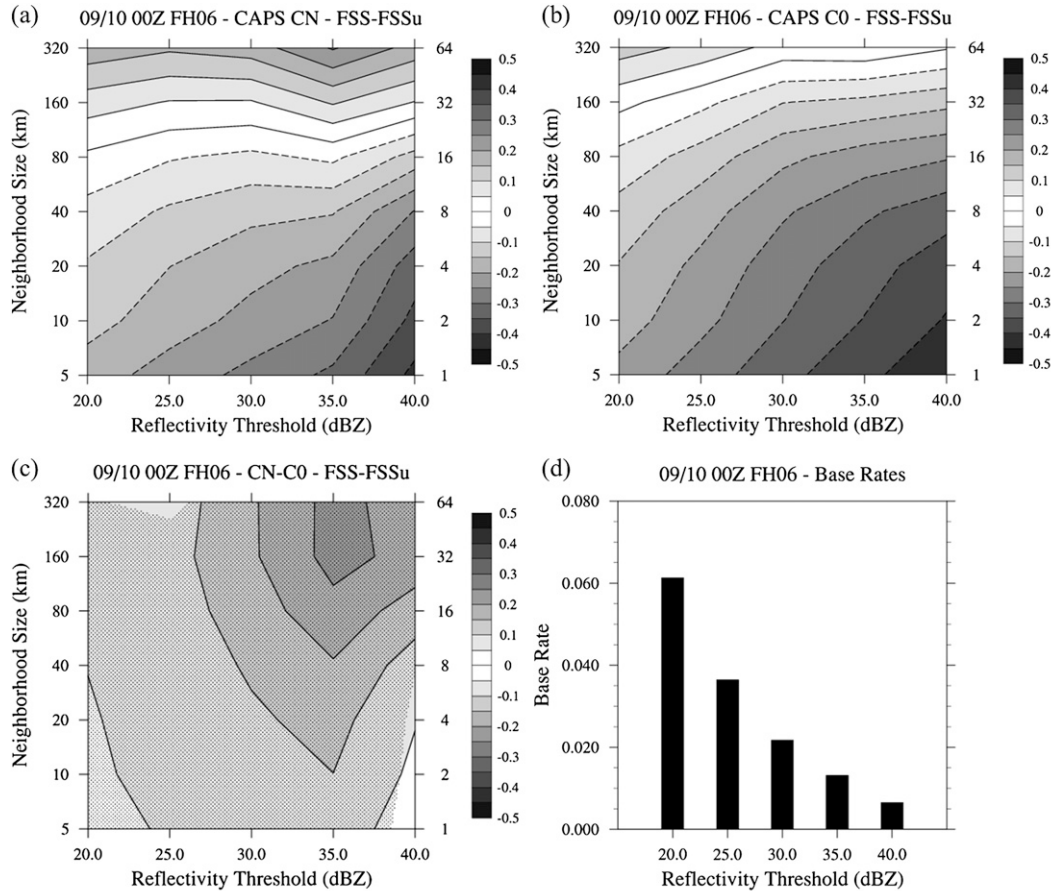


FIG. 11. As in Fig. 9, but for FH 6.

At FH 1, CN has no skill for both spatial scales less than about 40 km and thresholds greater than 25 dBZ (Fig. 13a). Thus, individual thunderstorms are not forecasted skillfully even after just 1 h of integration. A source of error at these scales could be related to the initialization procedure. Because the 3DVAR and cloud analyses are only performed at one time, there likely is not a dynamical balance between the 3DVAR wind field analysis that uses the radial winds in the Doppler radar data and the hydrometeor and in-cloud temperature and moisture adjustments from the cloud analysis that uses the reflectivity data (Hu et al. 2006b). As a result, the storms that are inserted into the initial conditions often undergo rapid adjustment, and new storms form along the outflow from the initial storms, or along boundaries and features that are either found in the initial conditions, or are inserted into the initial conditions by the 3DVAR analysis. C0 has positive skill for spatial scales greater than ~160 km for the lower reflectivity thresholds and for spatial scales greater than ~60 km for the higher reflectivity thresholds (Fig. 13b). The CN and C0 difference field reveals that CN performs better than C0

for all spatial scales and reflectivity thresholds at FH 1 (Fig. 13c), because C0 is still spinning up convection. Of significance is that CN overforecasts (high bias) for all spatial scales and reflectivity thresholds except for the highest thresholds (Fig. 13d), indicating that CN is generating too much convection in the first forecast hour. The spinup of convection in C0 is indicated by the negative ERD values for all spatial scales and reflectivity thresholds (Fig. 13e).

At FH 3, CN has no skill for both reflectivity thresholds greater than 30 dBZ and spatial scales less than ~80 km (Fig. 14a). Interestingly, a “tongue” of negative skill exists between the 40- and 80-km spatial scales for lower reflectivity thresholds. Positive skill exists on either side of this tongue. For C0, the tongue of negative skill exists between the spatial scales of 25 and 160 km (Fig. 14b). This region of positive skill on the small spatial scales in the plots is likely due to there being very few small-scale events with weak intensity, which causes only small errors compared to the random forecast at these scales (Casati 2010).

At FH 3, in the range of spatial scales from 40 to 320 km, CN is noticeably better than C0 at the lower

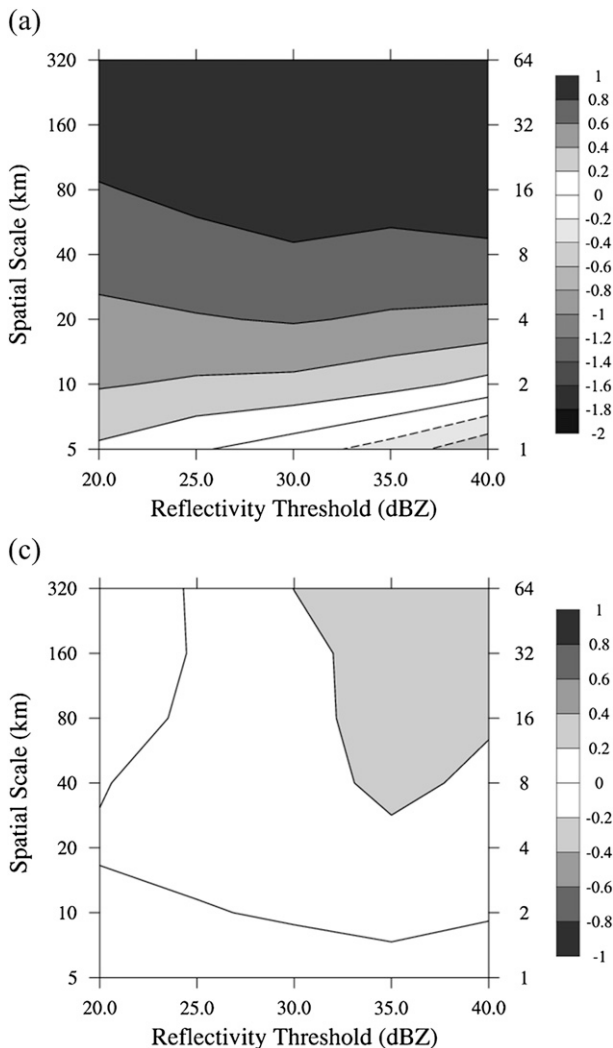


FIG. 12. (a) ISS and (b) ERD values for 2009 and 2010 for 0000 UTC CAPS CN at FH 0 for reflectivity thresholds every 5 dBZ from 20 to 40 dBZ and spatial scales from 5 to 320 km. Gray shading with solid contours in (a) represents positive skill, and gray shading with dashed contours in (a) represents negative skill. Gray shading with solid contours in (b) represents overforecasting, and gray shading with negative contours in (b) represents underforecasting. Values along the right ordinate represent multiples of the grid spacing.

reflectivity thresholds but not at 40 dBZ (Fig. 14c). The skill for CN appears to be better than for C0 at scales less than 40 km as well, but the significance is doubtful or nonexistent. This implies that CN has noticeably better skill in the near-term forecasting of precipitation than C0 down to 40-km spatial scales ($\sim 8\Delta x$). However, there is negative skill between the 40- and 80-km spatial scales for CN, so CN's improvement over C0 is only useful for spatial scales greater than ~ 80 km ($\sim 16\Delta x$). Once again, CN overforecasts for all spatial scales and for

reflectivity thresholds less than 35 dBZ (Fig. 14d). C0 continues to underforecast for reflectivity thresholds greater than 30 dBZ, but for reflectivity thresholds less than 30 dBZ, C0 has a small positive bias (Fig. 14e) as convection has spun up by this time.

At FH 6, the positive skill at the higher reflectivity thresholds seen at FH 3 remains the same for CN, but the positive skill for the lower thresholds between 80 and 160 km is lost (i.e., the region of negative skill shifts toward smaller reflectivities and larger scales) (Fig. 15a). The scales and thresholds of positive skill for C0 changed little from FH 3 to FH 6, except for the slight increase in positive skill for both small spatial scales and low reflectivity thresholds (Fig. 15b). The difference plot reveals that C0 has nearly "caught up" with CN for spatial scales less than ~ 40 km by FH 6 (Fig. 15c). This is consistent with the subjective impressions of the SFE2009 and SFE2010 participants, who tended to say CN and C0 were of nearly equal skill by FH 3–6. This suggests that the human participants were focusing not only on the higher reflectivity thresholds (see section 4a), but also on relatively small scales. In other words, they may have been rating CN and C0 more so based on smaller-scale convection (e.g., supercells), as opposed to larger-scale convective systems, which can have broad areas of high reflectivity (>35 dBZ).

However, an interesting result is that CN continues to show better skill than C0 for the spatial scales between ~ 40 and ~ 320 km. A possible reason why the spatial scales and reflectivity thresholds at which CN has positive skill and C0 has significantly lesser or negative skill is that the mesoscale convective systems and squall lines simulated by C0 tend to lag behind the observed systems more so than for CN. A comparison of the SR and OR beginning at 0000 UTC on 14 May 2009 illustrates this problem (Fig. 16). CN's simulated squall line largely overlaps the observed squall line after 6 h of integration, but C0's simulated squall line lags behind. This is a characteristic that was noticed on several days by the SFE2009 participants and was most clearly seen for squall lines and larger convective systems at greater than 30-dBZ thresholds. This shows that CN has difficulty retaining convective-scale skill (scales < 40 –80 km) through 3–6 h, but the information on the larger scales appears to be retained at and beyond 6 h and is manifest as convective systems with a smaller lag with observations compared to C0. With the initial data assimilation, CN has a better handle of the current state of the atmosphere on the larger scales with respect to latent heating and divergence. With that information, CN is able to maintain larger convective systems from the start, while C0 has to take time to develop that same convective system. Also at FH 6, CN continues to overforecast for

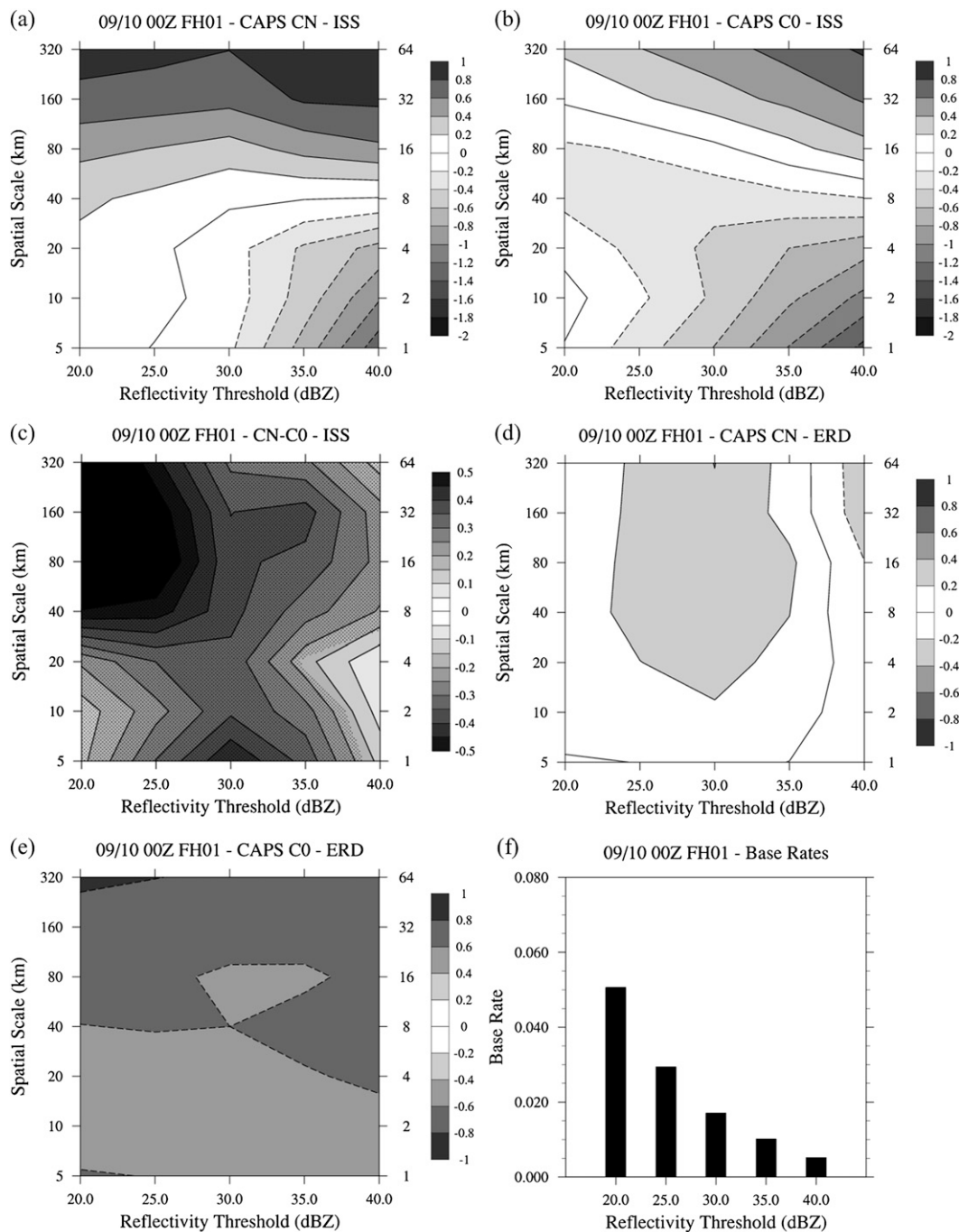


FIG. 13. ISS for 2009 and 2010 for 0000 UTC (a) CAPS CN and (b) CAPS C0 at FH 1 for reflectivity thresholds every 5 dBZ from 20 to 40 dBZ and spatial scales from 5 to 320 km. Gray shading with solid contours in (a) and (b) represents positive skill, and gray shading with negative contours in (a) and (b) represents negative skill. (c) ISS differences between CN and C0, where gray shading with solid contours represents $ISS_{CN} > ISS_{C0}$, gray shading with dashed contours (not depicted in these plots) represents $ISS_{CN} < ISS_{C0}$, and stippling represents 95% statistical significance. ERD values for (d) CN and (e) C0, where gray shading with solid contours represents overforecasting, and gray shading with dashed contours represents underforecasting. Values along the right ordinate represent multiples of the grid spacing. (f) Base rates of observed reflectivity for each threshold.

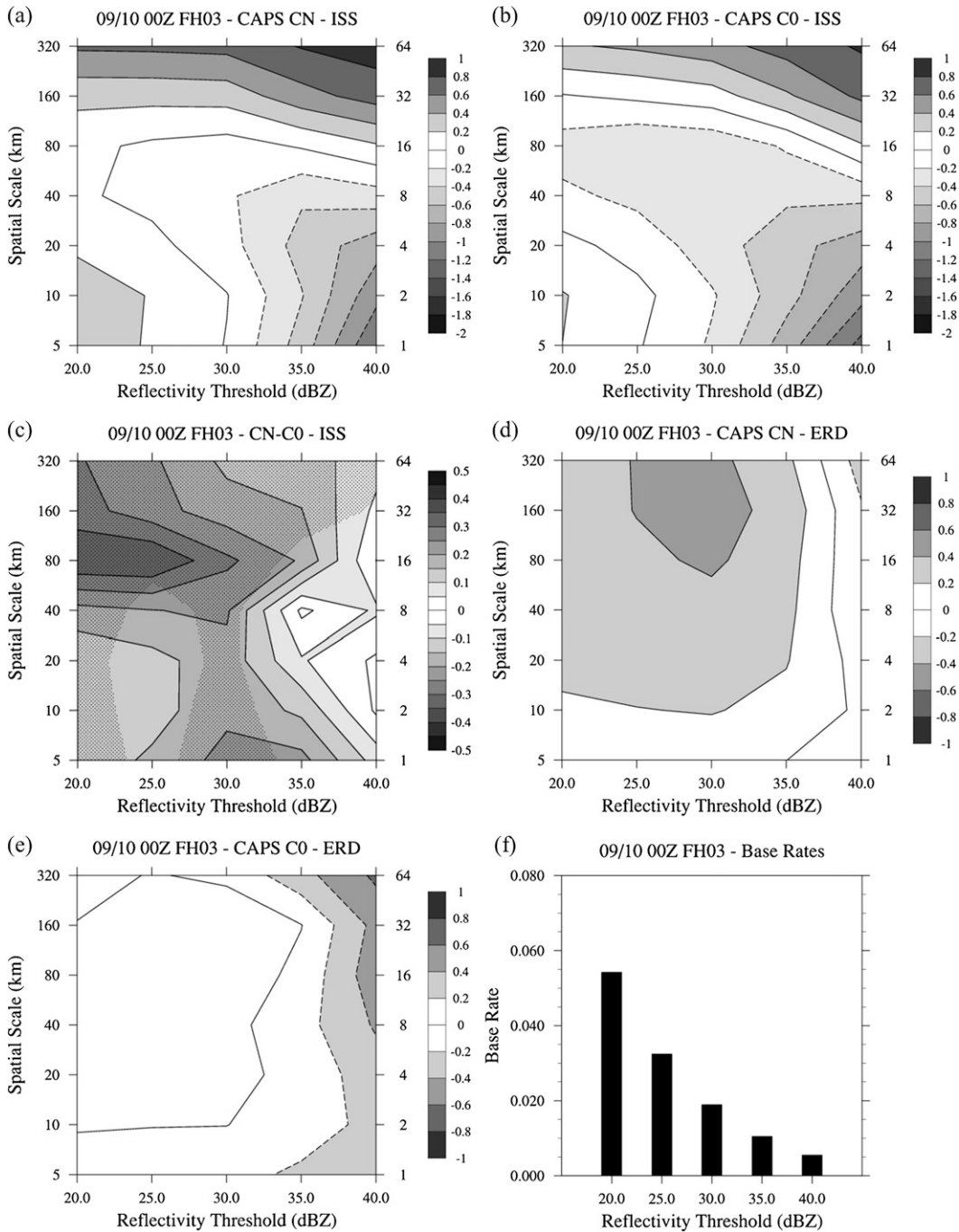


FIG. 14. As in Fig. 13, but for FH 3.

thresholds less than 35 dBZ, but now underforecasts for thresholds greater than 35 dBZ (Fig. 15d). C0 slightly overforecasts for small spatial scales and low reflectivity thresholds while underforecasting for thresholds greater than 35 dBZ, similar to CN (Fig. 15f), indicating that the spinup process in C0 is nearly complete. Forecast hours 9 and 12 depict similar results to FH 6 and are thus not shown.

5. Summary and conclusions

During a period of several weeks in the springs of the past several years, researchers and forecasters from across the country met in Norman, Oklahoma, for the annual Hazardous Weather Test Bed (HWT) Spring Forecasting Experiment to evaluate model forecasts from

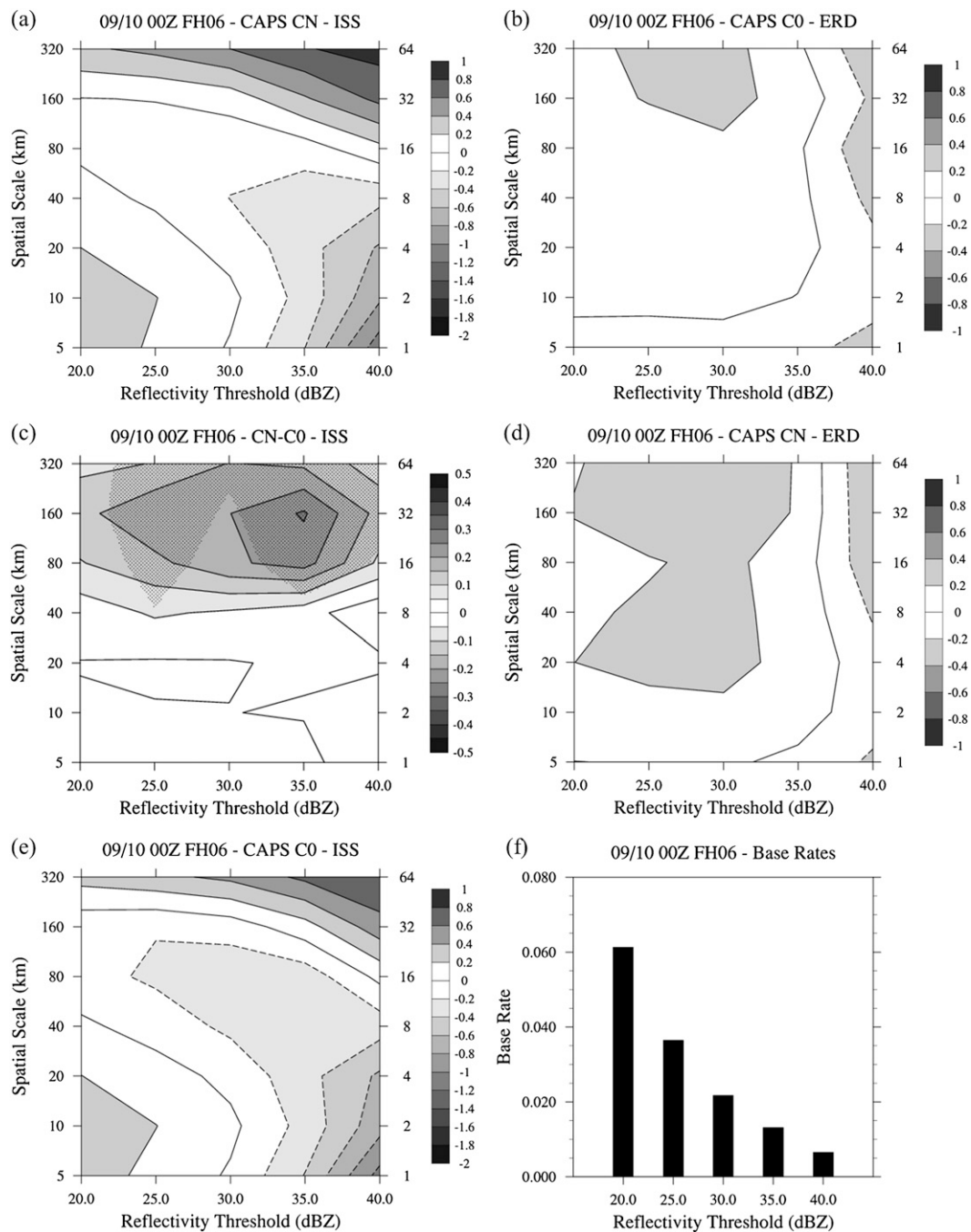


FIG. 15. As in Fig. 13, but for FH 6.

experimental storm-scale models. In 2009 and 2010, one of their tasks was to rate CN and C0 based on a visual inspection of the simulated and observed reflectivity. Most of the time, the participants noted that the skills of CN and C0 became roughly equivalent sometime between forecast hours 3 and 6. However, some traditional verification metrics, like GSS at lower thresholds, do not necessarily convey this message and can suggest that

beneficial information from radar is retained out to at least 12 h. As such, a main goal of this study was to determine if newer spatial verification techniques provide objective results that are qualitatively more similar to SFE2009 and SFE2010 participants' subjective assessment of the model forecasts than the traditional verification scores. Additionally, another important goal of this study was to evaluate the benefit of the 3DVAR-cloud

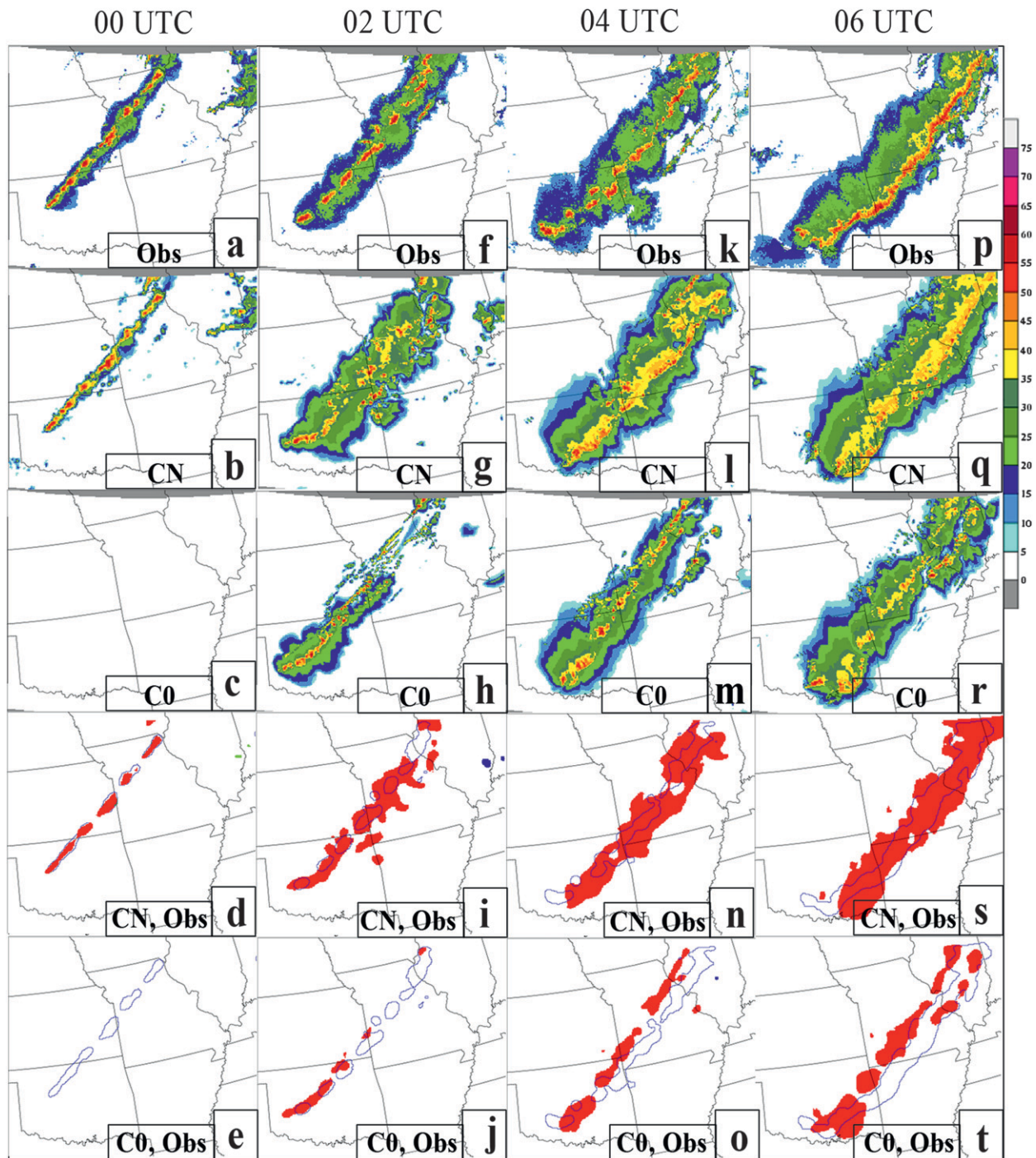


FIG. 16. First row is the observed composite reflectivity for (a) 0000, (f) 0200, (k) 0400, and (p) 0600 UTC 14 May 2009. Second and third rows are simulated reflectivity forecasts from 0000 UTC (b),(g),(l),(q) CAPS CN and (c),(h),(m),(r) CAPS C0 for the same times. In the bottom two rows, 30-dBZ thresholded observed reflectivity is marked by the thin blue line. Red shading represents 30-dBZ thresholded simulated reflectivity for (d),(i),(n),(s) CN and (e),(j),(o),(t) C0. From Kain et al. (2010).

analysis radar data assimilation technique, which was used in CN's forecasts.

To examine the reasons for the apparent discrepancy in subjective and objective metrics, and as part of an

objective assessment of the performance of CN and C0, several traditional verification metrics were computed for the CN and C0 forecasts of convection. It was found that the assessment of the relative performance of CN

versus C0 depends significantly on the metric of choice and on the chosen threshold of reflectivity (or, similarly, 1-h accumulated precipitation). According to the GSS (ETS), CN significantly outperformed C0 out to FH 6 (with doubtful significance out to FH 12, which does not agree well with the assessment from the Spring Forecasting Experiment participants) at the 20-dBZ threshold. However, at the 40-dBZ threshold, CN and C0's GSS scores converged after just a few hours of integration, which agrees much better with the sentiment of the SFE participants. This is likely due to the fact that the participants tended to focus on the higher reflectivities in the displays (the reflectivities with yellows and reds) rather than the weaker reflectivities (blues and greens). Also, CN's GSS scores at the 20-dBZ threshold were likely larger than C0's GSS due to CN's high-frequency bias, both in an absolute sense and relative to C0, for most thresholds.

In addition to the computation of traditional metrics, some new spatial verification techniques were used: the FSS computed using the neighborhood method was employed to assess the neighborhood and variable threshold combinations that yield useful forecasting skill for each forecast hour (Roberts and Lean 2008; Ebert 2008). Furthermore, the ISS computed from the scale-separation method was used to examine the error (MSE and bias) and skill on specific spatial scales (Casati 2010). These filtering methods serve to give credit to forecasts that are "close enough"; gridpoint-by-gridpoint metrics do not do so.

In general, both the FSS and the ISS show that CN lost most of its useful skill at neighborhood widths and spatial scales smaller than about 40 km ($8\Delta x$), and performs worse the higher is the threshold, after just a few hours of integration. As discussed in section 4c, a source of additional error at these widths and scales could be related to how there is likely not a dynamical balance between the 3DVAR wind field analysis and the hydrometeor and in-cloud temperature and moisture adjustments from the cloud analysis in the initialization procedure potentially resulting in rapid adjustments of storm coverage patterns. Even with this potential source of error, CN still performed better than C0, which has negative FSS for most neighborhood and threshold combinations through FH 6. Although, it is acknowledged that the Roberts and Lean "target skill" may not be optimal for the more convective precipitation events examined in this study possibly due to being too stringent.

The scale-separation method applied to the forecasts revealed many similar results compared to the neighborhood method, but there were some differences. For all forecast hours, a benefit of the 3DVAR analysis revealed clearly by the scale-separation method is seen in the larger spatial scales. The significant difference in ISS between CN and C0 for the 40–320-km spatial scales

and the lack of any significant differences at smaller spatial scales beyond a few hours shows that convective meso- γ and meso- β scales are contributing little to nothing to the improvement in skill seen for CN versus C0. A possible reason as to why this is the case was discussed in section 4c: mesoscale convective systems in C0 tend to lag behind the observed systems more so than for CN. This suggests that the information assimilated through the 3DVAR–cloud analysis system adds little to no skill at convective and smaller mesoscales (<40–80 km) starting at FH 1, but adds skill compared to a cold start at larger scales, even out to FH 12.

A goal of this work was to find objective measures of model skill that match the subjective impressions of experts that evaluated the models subjectively. It is found that the GSS for high reflectivity thresholds (>35 dBZ) matches subjective impressions that CN performed similarly to C0 by 3–6 h into the forecast, more so than lower thresholds (~20 dBZ). Furthermore, objective spatial verification metrics that examine model skill at scales less than 40–80 km match the subjective impressions as well. Therefore, these metrics (for these scales and thresholds) may be appropriate for use in providing an assessment consistent with experts' impressions of convection-allowing model forecast skill.

Furthermore, the two spatial filtering methods gave a more comprehensive characterization of the performance of the convection-allowing models than the traditional verification methods. The neighborhood and scale-separation methods revealed where "useful skill" might exist for several forecast hours in the reflectivity–spatial-scale parameter space that was not regularly apparent in the subjective evaluations or in the objective verification using the traditional scores. It is hoped that these results encourage future use of these new spatial verification metrics rather than the continued use of traditional verification metrics at single thresholds to characterize the performance of high-resolution, convection-allowing models. This is the first known study to appear in the refereed literature to use radar reflectivity instead of accumulated precipitation as the verification field for aggregate statistics computed over multiple seasons. It was found that both fields lead to similar results for all three verification methods discussed, giving confidence in the use of hourly simulated and observed reflectivity as a robust way to measure the performance of convection-allowing models. Finally, it would be beneficial to use these spatial verification metrics on case studies of convection or, perhaps, subsets of modes of convection (e.g., supercells versus disorganized multicells versus squall lines) aggregated together in order to not only verify model forecasts of convection, but also to study the different skill score structures associated with the various modes of convection.

Acknowledgments. This work was supported through NSSL and NOAA Earth System Research Laboratory's Global Systems Division (GSD) director's discretionary funds and through NOAA/Office of Oceanic and Atmospheric Research under NOAA–University of Oklahoma Cooperative Agreement NA08OAR4320904, U.S. Department of Commerce. Dr. Kim Elmore is thanked for his very helpful discussion of confidence intervals. Tara Jensen and everyone else associated with the use of MET at the DTC are thanked for their help in using MET. Drs. Jack Kain and Fred Carr are thanked for their insight into model verification. Model Evaluation Tools (MET) was developed at the National Center for Atmospheric Research (NCAR) through a grant from the U.S. Air Force Weather Agency (AFWA). NCAR is sponsored by the U.S. National Science Foundation. The CAPS forecasts were supported by the NOAA CSTAR grant to CAPS, and were produced at the National Institute of Computational Science (NICS) at the University of Tennessee, and at the Oklahoma Supercomputing Center for Research and Education (OSCER). Kevin Thomas and Fanyou Kong were instrumental in producing the forecasts.

REFERENCES

- Baldwin, M. E., and J. S. Kain, 2006: Sensitivity of several performance measures to displacement error, bias, and event frequency. *Wea. Forecasting*, **21**, 636–648.
- Casati, B., 2010: New developments of the intensity-scale technique within the Spatial Verification Methods Intercomparison Project. *Wea. Forecasting*, **25**, 113–143.
- , G. Ross, and D. B. Stephenson, 2004: A new intensity-scale approach for the verification of spatial precipitation forecasts. *Meteor. Appl.*, **11**, 141–154.
- , and Coauthors, 2008: Forecast verification: Current status and future directions. *Meteor. Appl.*, **15**, 3–18.
- Clark, A. J., and Coauthors, 2012: An overview of the 2010 Hazardous Weather Testbed Experimental Forecast Program Spring Experiment. *Bull. Amer. Meteor. Soc.*, **93**, 55–74.
- Doswell, C. A., III, R. Davies-Jones, and D. L. Keller, 1990: On summary measures of skill in rare event forecasting based on contingency tables. *Wea. Forecasting*, **5**, 576–585.
- DTC, 2011: MET: Version 3.0 Model Evaluation Tools users guide. Developmental Testbed Center, Boulder, CO, 209 pp. [Available at <http://www.dtcenter.org/met/users/docs/overview.php>.]
- Easterling, D. R., and P. J. Robinson, 1985: The diurnal variation of thunderstorm activity in the United States. *J. Climate Appl. Meteor.*, **24**, 1048–1058.
- Ebert, E. E., 2008: Fuzzy verification of high-resolution gridded forecasts: A review and proposed framework. *Meteor. Appl.*, **15**, 51–64.
- , 2009: Neighborhood verification: A strategy for rewarding close forecasts. *Wea. Forecasting*, **24**, 1498–1510.
- Elliot, A. J., and M. A. Maier, 2007: Color and psychological functioning. *Curr. Dir. Psychol. Sci.*, **16**, 250–254.
- Gilleland, E., D. Ahijevych, B. G. Brown, B. Casati, and E. E. Ebert, 2009: Intercomparison of spatial forecast verification methods. *Wea. Forecasting*, **24**, 1416–1430.
- , —, —, and E. E. Ebert, 2010: Verifying forecasts spatially. *Bull. Amer. Meteor. Soc.*, **91**, 1365–1373.
- Hamill, T. M., 1999: Hypothesis tests for evaluating numerical precipitation forecasts. *Wea. Forecasting*, **14**, 155–167.
- , and J. Juras, 2006: Measuring forecast skill: Is it real skill or is it the varying climatology? *Quart. J. Roy. Meteor. Soc.*, **132**, 2905–2923.
- Hu, M., M. Xue, and K. Brewster, 2006a: 3DVAR and cloud analysis with WSR-88D level-II data for the prediction of the Fort Worth, Texas, tornadic thunderstorms. Part I: Cloud analysis and its impact. *Mon. Wea. Rev.*, **134**, 675–698.
- , —, J. Gao, and K. Brewster, 2006b: 3DVAR and cloud analysis with WSR-88D level-II data for the prediction of the Fort Worth, Texas, tornadic thunderstorms. Part II: Impact of radial velocity analysis via 3DVAR. *Mon. Wea. Rev.*, **134**, 699–721.
- Kain, J. S., and Coauthors, 2010: Assessing advances in the assimilation of radar data and other mesoscale observations within a collaborative forecasting–research environment. *Wea. Forecasting*, **25**, 1510–1521.
- Lichtenfeld, S., M. A. Maier, A. J. Elliot, and R. Pekrun, 2009: The semantic red effect: Processing the word red undermines intellectual performance. *J. Exp. Soc. Psychol.*, **45**, 1273–1276.
- Mesinger, F., 2008: Bias adjusted precipitation threat scores. *Adv. Geosci.*, **16**, 137–142.
- Mittermaier, M., and N. Roberts, 2010: Intercomparison of spatial forecast verification methods: Identifying skillful spatial scales using the fractions skill score. *Wea. Forecasting*, **25**, 343–354.
- Roberts, N. M., and H. W. Lean, 2008: Scale-selective verification of rainfall accumulations from high-resolution forecasts of convective events. *Mon. Wea. Rev.*, **136**, 78–97.
- Schwartz, C. S., and Coauthors, 2009: Next-day convection-allowing WRF model guidance: A second look at 2-km versus 4-km grid spacing. *Mon. Wea. Rev.*, **137**, 3351–3372.
- Stephenson, D. B., B. Casati, C. A. T. Ferro, and C. A. Wilson, 2008: The extreme dependency score: A non-vanishing measure for forecasts of rare events. *Meteor. Appl.*, **15**, 41–50.
- Vasiloff, S. V., and Coauthors, 2007: Improving QPE and very short term QPF: An initiative for a community-wide integrated approach. *Bull. Amer. Meteor. Soc.*, **88**, 1899–1911.
- Wallace, J. M., 1975: Diurnal variations in precipitation and thunderstorm frequency over the conterminous United States. *Mon. Wea. Rev.*, **103**, 406–419.
- Wurman, J. D., C. A. Dowell III, Y. Richardson, P. Markowski, D. Burgess, L. Wicker, and H. Bluestein, 2012: The Second Verification of the Origin of Rotation in Tornadoes Experiment: VORTEX 2. *Bull. Amer. Meteor. Soc.*, **93**, 1147–1170.
- Xue, M., D.-H. Wang, J.-D. Gao, K. Brewster, and K. K. Droegemeier, 2003: The Advanced Regional Prediction System (ARPS) storm-scale numerical weather prediction and data assimilation. *Meteor. Atmos. Phys.*, **82**, 139–170.
- , and Coauthors, 2009: CAPS realtime multi-model convection-allowing ensemble and 1-km convection-resolving forecasts for the NOAA Hazardous Weather Testbed 2009 Spring Experiment. Preprints, *23rd Conf. on Weather Analysis and Forecasting/19th Conf. on Numerical Weather Prediction*, Omaha, NE, Amer. Meteor. Soc., 16A.2. [Available online at <http://ams.confex.com/ams/pdfpapers/154323.pdf>.]
- , and Coauthors, 2010: CAPS realtime storm scale ensemble and high resolution forecasts for the NOAA Hazardous Weather Testbed 2010 Spring Experiment. Preprints, *25th Conf. on Severe Local Storms*, Denver, CO, Amer. Meteor. Soc., 7B.3. [Available online at <https://ams.confex.com/ams/25SLS/webprogram/Paper176056.html>.]